Asian Journal of Chemistry; Vol. 32, No. 12 (2020), 3002-3006

ASIAN JOURNAL OF CHEMISTRY

https://doi.org/10.14233/ajchem.2020.22868

Doping Effect of Lead(II) on Structural and Optical Properties of Chromium Oxide Nanoparticles

N. KALAISELVI* and K.U. MADHU

Physics Research Centre, S.T. Hindu College (Affiliated to Manonmaniam Sundaranar University, Tirunelveli), Nagercoil-629002, India

*Corresponding author: E-mail: availnks84@gmail.com

Received: 20 June 2020; *Accepted*: 20 August 2020; *Published online*: 7 December 2020; AJC-20130

In this work, the effects of doping post transition metal (Pb^{2+}) on the structural, morphological, elemental and optical properties of pure chromium oxide nanoparticles are reported. The structural and morphological properties were examined by X-ray diffraction and scanning electron microscopy (SEM). The elemental composition of the prepared nanoparticles were estimated from energy dispersive X-ray (EDX) absorption spectra. The band gap energies of the prepared nanoparticles (4.72-3.78 eV) obtained from UV-vis absorption spectroscopy is higher than that of bulk Cr_2O_3 (3.3 eV), which ensures that the prepared nanoparticles were successfully synthesized in the nano-region.

Keywords: Chromium oxide nanoparticles, Doping, Lead(II) ions.

INTRODUCTION

Transition metal oxide nanoparticles have many applications in various fields [1]. In the midst of the transition metals, chromium oxide is an extensively used material. The foremost naturally occurring and highly stable form of chromium is the trivalent oxide. It has very low solubility and less reactivity which leads to low mobility in the environment and also possess low toxicity in living organisms. Chromium(III) oxide is used as a precursor for magnetic pigments. Because of its higher stability the trivalent oxide of chromium (Cr_2O_3) finds more refractory applications. Since it has ability to with stand at high temperature and highly resistive to corrosive conditions, chromium refractories are used in most severe environments [2]. Moreover, enormous number of publications related to the new applications of nano chromium oxide (Cr_2O_3) are reported [3]. Additionally the recent publications show that pigment field is one of the important fields which widely utilizes Cr_2O_3 [4-6], since it is used in paints and inks. Meanwhile chromium oxide (Cr_2O_3) can be used as a catalyst [7-10] and also extensively used in solar energy applications [11]. Chromium oxide (Cr_2O_3) films or coatings prevent metal and ceramics from corrosion and provides high wear resistance. Hence, the chromium oxide nanoparticles can be used in steel and ceramic industries [1,12]. Due to its multiple applications in various fields the researchers have made an attempt to prepare Cr_2O_3 nanoparticles by adopting different synthesis methods and reported their results [13].

Makhlouf *et al.* [14] prepared nanosized chromic oxide (Cr_2O_3) particles *via* chemical precipitation process. Likewise Cherian *et al.* [15] prepared Cr_2O_3 nanoparticles successfully through novel microwave technique method. Pei *et al.* [16] synthesized the Cr_2O_3 nanoparticles *via* hydrothermal synthesis in the reaction system of CrO_3 and HCHO aqueous solution. Hassen *et al.* [17] synthesized nano chromium oxide *via* sol-gel method, while Tsuzuki and McCormick [18] synthesized nano Cr_2O_3 *via* mechanochemical reaction procession. Bai *et al.* [19] prepared a cake-like Cr_2O_3 with a rhombohedral structure *via* microemulsion method. Anandan and Rajendran [20] have successfully produced the Cr_2O_3 nanoparticles *via* facile solvothermal method. Some other methods adapted to synthesis Cr_2O_3 nanoparticles are thermal decomposition and ball milling method [21,22]. Most of these synthesis methods have complications in being scaled up due to more complex process or expensive reaction apparatus. Herein, the synthesis and characterization of unadulterated Pb^{2+} doped chromium oxide nanoparticles using the simple and cheap microwave assisted solvothermal method are reported since it offers various advantages like efficient source of heating which increases the rate of reaction and enables faster synthesis.

EXPERIMENTAL

The chemicals *viz*. chromium triacetate, urea and lead acetate trihydrate were procured from Sigma-Aldrich, USA and used without further purification. Ethylene glycol was used as solvent. Double distilled water and acetone were used for washing the samples to remove the impurities.

Synthesis of chromium oxide nanoparticles: Chromium triacetate and urea were taken in the molecular ratio 1:3 and dissolved in 200 mL ethylene glycol using magnetic stirrer. Microwave irradiation was carried out till the solvent evaporated completely and a colloidal particles formed was washed several times with water followed with acetone to remove the impurities. The particles were dried in atmospheric air and then annealed at 700 ºC for 2 h. Similarly, Pb^{2+} doped Cr_2O_3 nanoparticles were prepared by adding lead acetate with the precursors used for the preparation of pure samples.

Characterization: The prepared samples were structurally characterized by X'Pert Pro-PAnalytic diffractometer with monochromated CuKα radiation (wavelength 1.5406 Å). The morphology of the pure and Pb^{2+} doped samples have been unveiled with SEM images obtained from scanning electron microscopy (Jeol, Japan). The atomic weight percentage of the elements found in the pure and Pb^{2+} doped samples were obtained from EDX spectra recorded by Oxford instruments, UK. The optical absorbance spectrum of pure and Pb^{2+} doped Cr_2O_3 nanoparticles were taken by Perkin-Elmer UV WinLab 6.0.4.0738/1.61.00 Lambda 900.

RESULTS AND DISCUSSION

PXRD analysis: The synthesized pure and doped Cr_2O_3 nanoparticles are subjected to PXRD analysis using X'Pert Pro-P Analytic diffractometer with monochromated CuKα radiation (wavelength 1.5406 Å) at high generator voltage (40 KV), in the angular range 20-80º of 2θ. The XRD patterns of pure and different concentration of Pb^{2+} doped sample are shown in Fig. 1. The occurrence of intense and sharp peaks and the absence of diffraction halo, indicate the formation of high crystalline phase of the proposed samples and with absence of amorphous phase formation. Furthermore, the *d*-spacing got for unadulterated Cr_2O_3 concur well with that of reported one in JCPDS file 82-1484, it belongs to rhombohedral system with lattice parameter $a = 4.957$; $c = 13.592$ and space group $R\bar{3}c$. When compared with JCPDS diffraction peaks, the present diffraction pattern shows a slight shift in diffraction angles along with intensity variation. This may due to the effect of crystallite size and lattice strain [23]. The presence of these

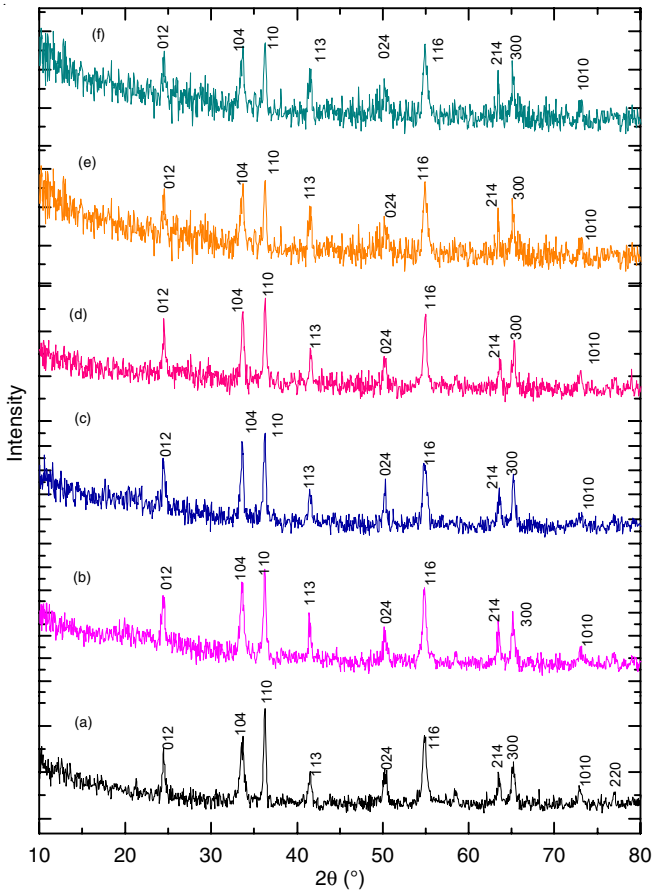

Fig. 1. PXRD pattern of pure and Pb^{2+} doped Cr_2O_3 nanoparticles (a) pure Cr_2O_3; nanoparticles; (b) 2 wt %; (c) 4 wt %; (d) 6 wt %; (e) 8 wt %; and (f) 10 wt % Pb^{2+} doped Cr_2O_3 nanoparticles

shift may also recognized with the contrast between the ionic radii of the substitute Pb^{2+} (1.19 Å) with that of Cr^{3+} (0.64 Å), These outcomes are anomalous proof to demonstrate the way that a portion of Cr^{3+} particles have been displaced by dopant particles. The lattice parameters (*a* and *c*) of the pure and Pb^{2+} doped Cr_2O_3 nanoparticles are calculated from the following equation [24]:

$$\frac{1}{d^2} = \frac{4}{3}\left(\frac{h^2 + hk + k^2}{a^2}\right) + \frac{l^2}{c^2}$$

The variation of *a* and *c* with dopant concentration revealed that added dopants successfully entered in Cr_2O_3 lattice and produce lattice elongation. Thus the dopant induces a strain in Cr_2O_3 parent lattice. The average grain size listed in Table-1 was calculated from Debye-Scherrer method [25-28]. The reason

TABLE-1
STRUCTURAL DATA OBTAINED FROM XRD PATTERNS OF PURE AND Pb^{2+} DOPED Cr_2O_3 NANOPARTICLES

Sample name	Dopant concentration (wt %)	Lattice parameter		Unit cell volume	Grain size (error~ ±2)
		a	c		Scherrer method (nm)
Pure Cr_2O_3		4.9573	13.6138	334.5567	24.4
Cr_2O_3: Pb	2	4.9612	13.6287	335.4501	25.7
	4	4.9731	13.6354	337.2269	27.3
	6	4.9754	13.6458	337.7964	27.6
	8	4.8125	13.6411	315.9300	28.0
	10	4.8741	13.6574	324.4568	29.3

for increase in grain size of Cr_2O_3 after Pb^{2+} doping may due to the difference in atomic radius; this may increase the tendency for the agglomeration and produce larger grain size. The average grain size obtained for pure and the doped samples were small when compared with other reported values [11,29-32].

SEM analysis: The morphology of unadulterated and Pb^{2+} doped Cr_2O_3 nanoparticles having spherical shape and higher degree of agglomeration were recorded with scanning electron microscope for all the prepared samples and are shown in Fig. 2. The spherical nanoparticles were agglomerated to reduce the entire surface free vitality. It can likewise be seen that the surface morphology of the nanoparticles did not indicate an appreciable change in Pb^{2+} doping.

It was reported that the shape of the prepared nanoparticles formed due to aggregation is an undefined one, while the shape of particles produced by agglomeration is generally spherical [33-35]. In the present investigation, ethylene glycol is used as a solvent since it acts as a good reducing agent and reduces the particle size to a greater extent. It was reported that organic solvents endorse the formation of spheres and rods [36], consequently an analogous trend was noticed with ethylene glycol too. Since the prepared nanoparticles are so small, they are very unstable and tend to agglomerate.

EDAX analysis: Energy dispersive X-ray spectra (EDX) of the pure and Pb^{2+} doped Cr_2O_3 nanoparticles are shown in Fig. 3. The solid pinnacles of Cr and O were plainly present in the range and no indications of dissimilar compounds were seen in the spectra proved the virtue of the samples. As the dopant concentration increases the height of the peak also increases, it proves that the dopant has entered in to the lattice. The gold peak was formed around 2.2 keV since it is used as a coating material to increase the conductivity. The peaks due to carbon around 0.27 keV are assigned to the carbon coated layer.

UV-vis analysis: From Fig. 4, it is observed that the absorption peak on set is red shifted with the increasing concentration of Pb^{2+} from 2 wt % to 10 wt %. But the shifting is non-systematic with concentration of dopants. The red shift of Pb^{2+} doping may be due to surface plasma effect and also denotes weak confinement due to aggregation of nanoparticles.

The curves were plotted between $(\alpha h\nu)^2$ *versus* $(h\nu)$ and extrapolating of the linear portions of the curves to the $h\nu$ axis gives E_g (Fig. 5). It is clearly observed that the band gap of Pb^{2+} doped Cr_2O_3 nanoparticles decreases non-systematically from 4.72 eV (pure) to 3.78 eV (10 wt. % Pb^{2+}doped Cr_2O_3), which are higher than that of the bulk (3.4 eV), provides the evidences of the quantum confinement effect. In fact, the band gaps of bulk particles are actually formed by the unification of a bunch of adjacent energy levels with a huge number of atoms and molecules. When the particle size reaches the nano scale, the number of atoms and molecules present in every particle is largely reduced. The width of the band gap gets narrower due to the reduction of the number overlapping of orbitals or energy levels. This is the origin of increase in energy band gap between the valency band and the conduction band. It is the reason behind the higher energy gap in nanoparticles than in the equivalent bulk matter. Hence, the nanoparticles have lower electrical conductivity when compared with bulk particles from which they are synthesized. Accordingly there is a shift produced in the absorption spectrum towards the lower wavelength or blue region. The decrease in E_g for Pb^{2+} doped samples is due to increase in crystallite size from 24.4 nm to 29.3 nm (10 wt % Pb^{2+} doped Cr_2O_3) as the result of incorporation of Pb^{2+} ions with comparable radius to that of Cr^{3+} ions. The observed E_g value of pure Cr_2O_3 nanoparticle (4.72 eV) is higher than that of the energy band gap value (4.04 eV) as reported by Anandan *et al.* [32] and enormously higher than

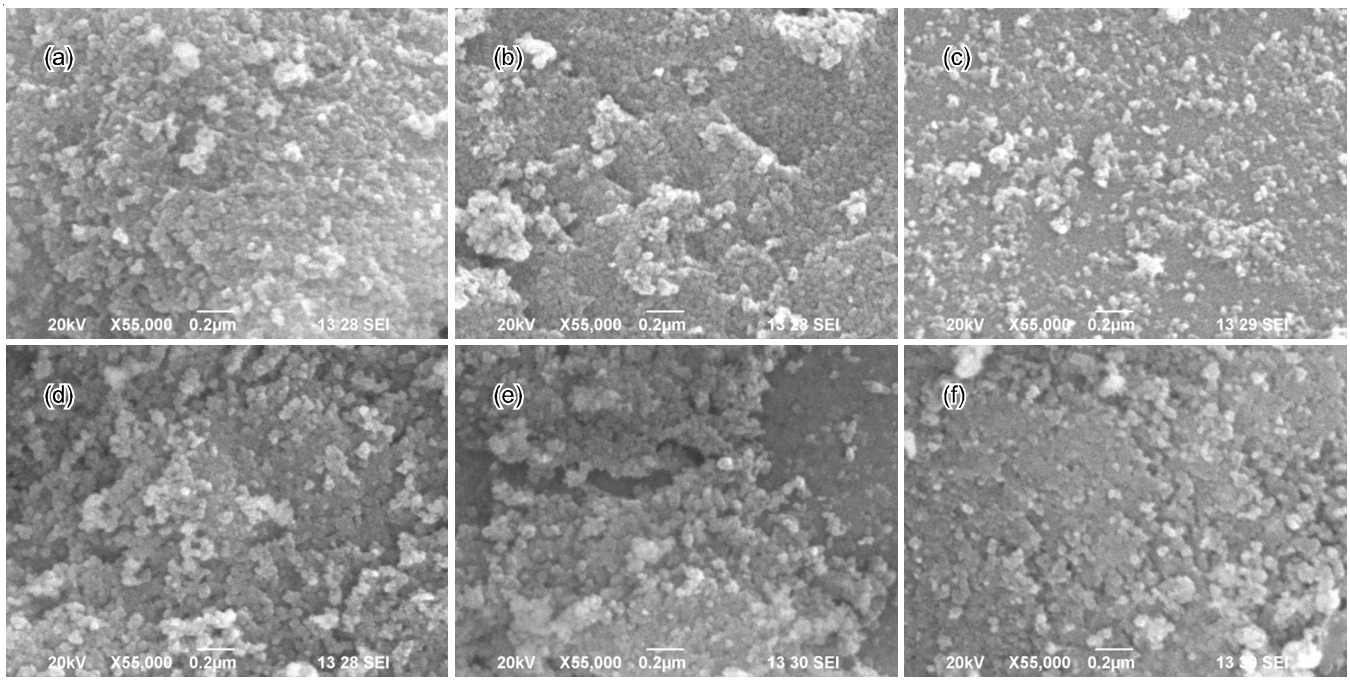

Fig. 2. SEM images of (a) pure Cr_2O_3 nanoparticles; (b) 2 wt %; (c) 4 wt %; (d) 6 wt %; (e) 8 wt %; and (f) 10 wt % Pb^{2+} doped Cr_2O_3 nanoparticles

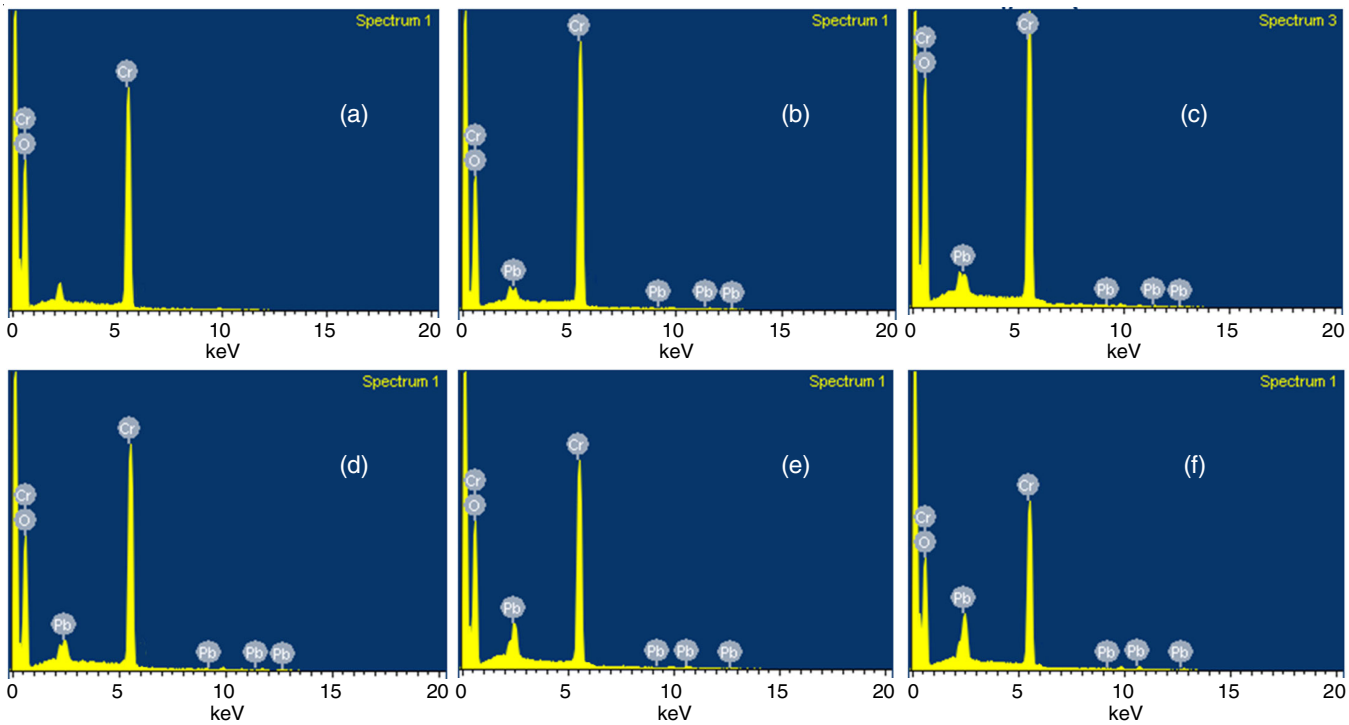

Fig. 3. EDX spectrum of (a) pure Cr_2O_3 nanoparticles; (b) 2 wt %; (c) 4 wt %; (d) 6 wt %; (e) 8 wt %; and (f) 10 wt % Pb^{2+} doped Cr_2O_3 nanoparticles

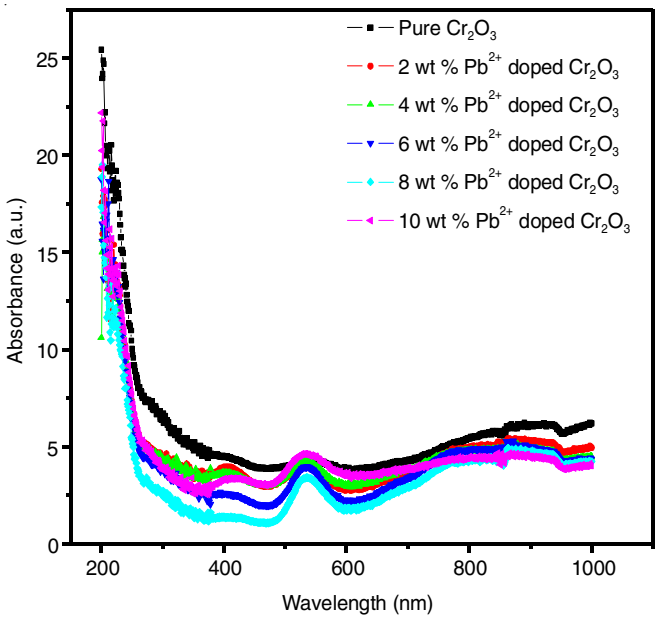

Fig. 4. UV-vis absorbance spectra of pure and different concentration of Pb^{2+} doped Cr_2O_3

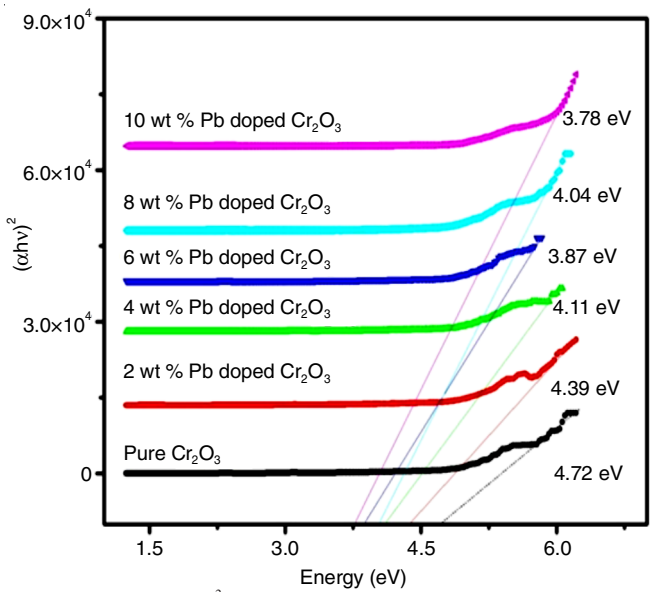

Fig. 5. Graph of $(\alpha h\nu)^2$ as a function of photon energy ($h\nu$) for different concentration of Pb doped Cr_2O_3 nanoparticles

the reported value of (3.164 eV) for Cr_2O_3 nanoparticles [37]. The energy bandgap of Cr_2O_3 nanoparticles prepared by thin film techniques [38-40] is also lower than the band gap values of pure and Pb^{2+} doped Cr_2O_3 nanoparticles prepared by microwave assisted solvothermal method. This discrepancy in the band gap may be explained on the basis of morphology and size effect of prepared nanoparticles [41]. This wider band gap material is commonly used in UV-light emitters and optical storage devices [42].

Conclusion

This study reported the synthesis and characterization of pure and Pb^{2+} doped chromium oxide nanoparticles possess rhombohedral structure with particle size varied from 24.4-29.3 nm. SEM determines the spherical and slightly agglomerated morphology of the obtained nanoparticles. EDX reveals the presence of expected elements in the synthesized nanoparticles. The variation of band gap on doping Pb^{2+} with pure chromium oxide was clearly observed and greater than that of a bulk chromium oxide, which confirms the quantum confinement.

CONFLICT OF INTEREST

The authors declare that there is no conflict of interests regarding the publication of this article.

REFERENCES

1. Z. Pei, X. Zheng and J. Zhiguo Li, *Nanosci. Nanotechnol.*, **16**, 4655 (2016).
2. J. Barnhart, *Regul. Toxicol. Pharmacol.*, **26**, S3 (1997); https://doi.org/10.1006/rtph.1997.1132
3. P.M. Sousa, A.J. Silvestre and O. Conde, *Thin Solid Films*, **519**, 3653 (2011); https://doi.org/10.1016/j.tsf.2011.01.382
4. M.J. Derelanko, W.E. Rinehart, R.J. Hilaski, R.B. Thompson and E. Loser, *Toxicol. Sci.*, **52**, 278 (1999); https://doi.org/10.1093/toxsci/52.2.278
5. E. Ozel and S. Turan, *J. Eur. Ceram. Soc.*, **23**, 2097 (2003); https://doi.org/10.1016/S0955-2219(03)00036-0
6. Li, Z.F. Yan, G.Q. Lu and Z.H. Zhu, *J. Phys. Chem. B*, **110**, 178 (2006); https://doi.org/10.1021/jp053810b
7. J.F. Ma, J.F. Ding, L.M. Yu, L.Y. Li, Y. Kong and S. Komarneni, *Appl. Clay Sci.*, **107**, 85 (2015); https://doi.org/10.1016/j.clay.2015.01.007
8. Rafi-ud-din, Q. Xuanhui, L. Ping, L. Zhang, W. Qi, M.Z. Iqbal, M.Y. Rafique, M.H. Farooq and Islam-ud-din, *J. Phys. Chem. C*, **116**, 11924 (2012); https://doi.org/10.1021/jp302474c
9. M.K. Bates, Q.Y. Jia, N. Ramaswamy, R.J. Allen and S. Mukerjee, *J. Phys. Chem. C*, **119**, 5467 (2015); https://doi.org/10.1021/jp512311c
10. S. Karuppuchamy, H. Matsui, K. Kira, M.A. Hassan and M. Yoshihara, *Ceram. Int.*, **38**, 1515 (2012); https://doi.org/10.1016/j.ceramint.2011.09.035
11. S. Khamlich, O. Nemraoui, N. Mongwaketsi, R. Mccrindle, N. Cingo and M. Maaza, *Physica B*, **407**, 1509 (2012); https://doi.org/10.1016/j.physb.2011.09.073
12. J. Ouyang and S. Sasaki, *Wear*, **249**, 56 (2001); https://doi.org/10.1016/S0043-1648(01)00530-0
13. T. Iqbal, S. Tufail and S. Ghazal, *Int. J. Nanosci. Nanotechnol.*, **13**, 19 (2017).
14. S.A. Makhlouf, Z.H. Bakr, H. Al-Attar and M.S. Moustafa, *Mater. Sci. Eng. B*, **178**, 337 (2013); https://doi.org/10.1016/j.mseb.2013.01.012
15. M. Cherian, M.S. Rao, S.S. Manoharan, A. Pradhan and G. Deo, *Top. Catal.*, **18**, 225 (2002); https://doi.org/10.1023/A:1013838621968
16. Z.Z. Pei and Y. Zhang, *Mater. Lett.*, **62**, 504 (2008); https://doi.org/10.1016/j.matlet.2007.05.073
17. A. Hassen, A.M. El Sayed, W.M. Morsi and S. El-Sayed, *J. Appl. Phys.*, **112**, 093525 (2012); https://doi.org/10.1063/1.4764864
18. T. Tsuzuki and P.G. McCormick, *Acta Mater.*, **48**, 2795 (2000); https://doi.org/10.1016/S1359-6454(00)00100-2
19. G.M. Bai, H.X. Dai, Y.X. Liu, K.M. Ji, X.W. Li and S.H. Xie, *Catal. Commun.*, **36**, 43 (2013); https://doi.org/10.1016/j.catcom.2013.02.025
20. K. Anandan and V. Rajendran, *Mater. Sci. Semicond. Process.*, **19**, 136 (2014); https://doi.org/10.1016/j.mssp.2013.12.004
21. O. Jankovsky, D. Sedmidubsky, Z. Sofer, J. Luxa and V. Bartunek, *Ceram. Int.*, **41**, 4644 (2015); https://doi.org/10.1016/j.ceramint.2014.12.009
22. P. Hajra, P. Brahma, S. Dutta, S. Banerjee and D. Chakravorty, *J. Magn. Magn. Mater.*, **324**, 1425 (2012); https://doi.org/10.1016/j.jmmm.2011.11.064
23. V. Balouria, A. Singh, A.K. Debnath, A. Mahajan, R.K. Bedi, D.K. Aswal and S.K. Gupta, *AIP Conf. Proc.*, **1447**, 341 (2012); https://doi.org/10.1063/1.4710019
24. S.F. Shayesteh and A.A. Dizgah, *Pramana-J. Phys.*, **81**, 319 (2013).
25. S.A. Makhlouf, M.A. Kassem and M.A. Abdel-Rahim, *J. Mater. Sci.*, **44**, 3438 (2009); https://doi.org/10.1007/s10853-009-3457-0
26. M.M. Abdullah, F.M. Rajab and S.M. Al-Abbas, *AIP Adv.*, **4**, 027121 (2014); https://doi.org/10.1063/1.4867012
27. F. Talavari, A. Shakeri and H. Mighani, *J. Environ. Anal. Chem.*, **5**, 231 (2018); https://doi.org/10.4172/2380-2391.1000231
28. P. Jayamurugan, R. Mariappan, K. Premnazeer, S. Ashokan, Y.V. Subba Rao, N.V.S.S. Seshagiri Rao and C. Shanmugapriya, *Sens. Imaging*, **18**, 22 (2017); https://doi.org/10.1007/s11220-017-0170-y
29. Ritu, *IOSR J. Appl. Chem.*, **8**, 5 (2015).
30. V.S. Jaswal, A.K. Arora, M. Kinger, V.D. Gupta and J. Singh, *Orient. J. Chem.*, **30**, 559 (2014); https://doi.org/10.13005/ojc/300220
31. R. Meenambika, R. Ramalingom and T.C. Thanu, *Eng. Res. Appl.*, **4**, 20 (2014).
32. K. Anandan and V. Rajendran, *Mater. Sci. Semiconduct. Process.*, **19**, 136 (2014); https://doi.org/10.1016/j.mssp.2013.12.004
33. G.Z. Wang, R. Saeterli, P.M. Rorvik, A.T.J. van Helvoort, R. Holmestad, T. Grande and M.A. Einarsrud, *Chem. Mater.*, **19**, 2213 (2007); https://doi.org/10.1021/cm063047d
34. M.O. Olderoy, M.L. Xie, B.L. Strand, E.M. Flaten, P. Sikorski and J.P. Andreassen, *Cryst. Growth Des.*, **9**, 5176 (2009); https://doi.org/10.1021/cg9005604
35. J.M. Kim, S.M. Chang, J.H. Chang and W.S. Kim, *Colloids Surf. A Physicochem. Eng. Asp.*, **384**, 31 (2011); https://doi.org/10.1016/j.colsurfa.2011.03.016
36. L. Xu, Y.L. Hu, C. Pelligra, C.-H. Chen, L. Jin, S. Sithambaram, H. Huang, M. Aindow, R. Joesten and S.L. Suib, *Chem. Mater.*, **21**, 2875 (2009); https://doi.org/10.1021/cm900608d
37. K. Mohanapandiana and A. Krishnan, *Int. J. Adv. Eng. Technol.*, **7**, 273 (2016).
38. M.F. Al-Kuhaili and S.M.A. Durrani, *Opt. Mater.*, **29**, 709 (2007); https://doi.org/10.1016/j.optmat.2005.11.020
39. A. Ji, W. Wang, G.H. Song, Q.M. Wang, C. Sun and L.S. Wen, *Mater. Lett.*, **58**, 1993 (2004); https://doi.org/10.1016/j.matlet.2003.12.029
40. C.H. Lin, S.Y. Chen and P. Shen, *J. Phys. Chem. C.*, **113**, 16356 (2009); https://doi.org/10.1021/jp904288n
41. M. Singh, M. Goyal and K. Devlal, *J. Taibah Univ. Sci.*, **12**, 470 (2018); https://doi.org/10.1080/16583655.2018.1473946
42. H. Cao, X. Qiu, Y. Liang, M. Zhao and Q. Zhu, *Appl. Phys. Lett.*, **88**, 241112 (2006); https://doi.org/10.1063/1.2213204